1 # Accuracy of wind observations from open-ocean buoys:

2 # Correction for flow distortion

3 Michael Schlundt[1,*], J. Thomas Farrar[1], Sebastien P. Bigorre[1], Albert J. Plueddemann[1],

4 Robert A. Weller[1]

5 [1] Woods Hole Oceanographic Institution, Woods Hole, MA, USA

6 * Now at: GEOMAR Helmholtz Centre for Ocean Research Kiel, Kiel, Germany

7

8 Correspondence to: M. Schlundt (mschlundt@geomar.de)

9

10 **Abstract**

11 The comparison of equivalent neutral winds obtained from (a) four WHOI buoys in the

12 subtropics and (b) scatterometer estimates at those locations reveals a root-mean-square

13 (RMS) difference of 0.56-0.76 m/s. To investigate this RMS difference, different buoy wind

14 error sources were examined. These buoys are particularly well suited to examine two

15 important sources of buoy wind errors because: (1) redundant anemometers and a

16 comparison with numerical flow simulations allow us to quantitatively assess flow distortion

17 errors, and (2) one-minute sampling at the buoys allows us to examine the sensitivity of buoy

18 temporal sampling/averaging in the buoy-scatterometer comparisons. The inter-

19 anemometer difference varies as a function of wind direction relative to the buoy wind vane

20 and is consistent with the effects of flow distortion expected based on numerical flow

21 simulations. Comparison between the anemometers and scatterometer winds supports the

22   interpretation that the inter-anemometer disagreement, which can be up to 5% of the wind

23   speed, is due to flow distortion. These insights motivate an empirical correction to the

24   individual anemometer records and subsequent comparison with scatterometer estimates

25   show good agreement.

26

2

1. Introduction

Knowledge of the global wind field is crucial for modeling societally important oceanographic phenomena, such as ocean currents, surface waves, and regional climate modes such as El Niño. During the last four decades several global wind observation data sets have become available from satellites using radiometers and scatterometers. All of them have in common the fact that they do not observe the wind, but instead measure related parameters like brightness temperature or backscattered radiation. These parameters are related to the small-scale surface roughness, which is in turn related to the surface stress, and are finally converted to winds via a geophysical model function (GMF). For the development of the GMF, direct in-situ observations are essential; and observations from buoys are critical for providing a baseline for winds over the open ocean.

The characterization of errors in in-situ measurements is critical to understanding wind-driven processes as well as evaluating remotely sensed winds from satellite. Error sources are myriad, but here are grouped into three main categories: errors inherent to the instrument, errors associated with the platform, and sampling errors. The accuracy of the measurement is dependent on sensor accuracy, sensor location, and sampling methodologies. Sensor errors are usually estimated and provided by the manufacturer. Platform related errors are of particular interest because they often result in measurement bias. These biases are related to the performance of the sensor in the deployed environment; hence, for wind sensors on a buoy at the ocean surface there can be, for example, compass errors due to the local magnetic field or flow distortion caused by the buoy superstructure. Sampling errors can arise

3

49   from incomplete sampling of the measured parameter, and can be caused by discrete

50   sampling or by the spatial or temporal averaging that is inherent in a measurement

51   technique.

52

53   This paper focuses on understanding the performance of wind sensors on surface buoys. The

54   Woods Hole Oceanographic Institution (WHOI) Upper Ocean Processes (UOP) Group has

55   maintained several moored buoys in the Pacific and Atlantic Ocean for almost two decades.

56   The buoys used in this study are well maintained and are equipped with redundant

57   meteorological instruments. The temporal resolution of the meteorological data is one

58   minute, and the measurement height is about three meters above the sea surface on the

59   buoy tower. In the case of wind measurements, a minimum of two anemometers are

60   mounted on the buoys. Colbo and Weller (2009) analyzed and described the errors from the

61   wind observations made on UOP buoys. The precision of the wind speed sensor is 0.002 m/s

62   with a total error 0.1 m/s. The wind direction measurement has a precision of 0.1° and a total

63   instant error of about 6°. Both total errors can be higher for very low wind speed conditions.

64

65   A large vane is fixed to the leeward side of the tower on the buoy with the intention of

66   controlling the orientation of the buoy with respect to the wind and keeping the forward face

67   of the tower, where anemometers and temperature and humidity sensors are mounted,

68   facing into the wind. It is notable that deployments showed a bi-stable orientation of the

69   buoy, tending to divert about 30° in either direction from the head-on wind, indicating that

70   the vane on the tower did not steer the forward face of the buoy tower directly into the wind.

4

71   Opposing the steering action of the vane are the wind forces on the tower structure and the

72   sensors and also on the watertight storage well in the center of the buoy which houses

73   batteries and data loggers; the top of the well extends about 15 cm above the buoy deck and

74   is covered by a hatch.

75

76   As part of the quality control work on the buoy data, observations from the redundant

77   anemometers of each buoy are compared, and some differences have been noted. A

78   computational fluid dynamics (CFD) study of the buoy type that the UOP group has been using

79   since around 2004 (Emond et al. 2012) suggested the two anemometers could disagree by up

80   to 5% of the wind speed. This CFD study also revealed an asymmetry in wind speeds of the

81   port and starboard sensors, when investigating the flow distortion with oblique winds.

82   However, it has to be mentioned that the CFD simulations were done for an idealized setting,

83   with no wave motion or tilt on the buoy. An experiment in the Gulf Stream showed wind

84   speed and direction discrepancies between sensors at different locations on the buoy tower

85   consistent with the predictions of the flow distortion study, and it also showed a dependence

86   of the inter-anemometer disagreement on the angle between the wind and the buoy's wind

87   vane (Bigorre et al. 2013).

88

89   To quantify biases and to bring the results in relation to other wind observations, the buoy

90   observations were compared with two scatterometer datasets. Scatterometers have many

91   sources of wind measurement biases that are well documented (e.g., Stoffelen and Portabella

92   2006; De Kloe et al. 2017; Verhoef et al. 2017). However, these biases are not believed to be

5

93   variable on a global scale, i.e. they are relatively stable over the investigated analysis period

94   (Ricciardulli and Wentz 2015), a property we will exploit here to get further insights into the

95   buoy errors caused by flow distortion.

96

97   The first scatterometer we use, operational from 1999 until 2009 in Ku-band, is NASA

98   QuikSCAT (Lungu and Callahan 2006) with its most current GMF: 'QuikSCAT Ku-2011'

99   (Ricciardulli and Wentz 2015). Neglect of an SST dependency in the wind-stress relationship

100   can be a large error source (see e.g., Wang et al. 2017). Generally, pencil-beam

101   scatterometers, like QuikSCAT, can have systematic wind direction biases, as shown e.g. by

102   Stoffelen and Portabella (2006). The second scatterometer is ASCAT, which is an EUMETSAT

103   project and operating in C-band (Figa-Saldaña et al. 2002). This frequency band is less

104   influenced by rain than the Ku-band (Weissman et al. 2012). Currently, three ASCAT (ASCAT-

105   A, ASCAT-B, and ASCAT-C) scatterometers are in orbit.

106

107   The differences between scatterometer and in-situ wind speeds on regional scales can be

108   large for both described scatterometer missions. Ricciardulli and Wentz (2015) estimated a

109   root-mean-square (RMS) difference for 30-min collocations over 5 years between the used

110   QuikSCAT dataset and a variety of buoys of 0.87 m/s with only a marginal bias of -0.03 m/s.

111   For ASCAT they estimated a RMS of 1.11 m/s with no bias (-0.01 m/s). A few publications

112   provided RMS differences as well. Yu and Jin (2012) found a RMS of 0.66 m/s for the whole

113   QuikSCAT period using a large set of daily-averaged buoy observations. Freilich and Dunbar

114   (1999) found an RMS disagreement of 1.3 m/s using the NASA scatterometer (NSCAT) and

6

115   hourly observations of National Data Buoy Center (NDBC) buoys. Ebuchi, Graber and Caruso

116   (2002) used almost one and a half years of QuikSCAT observations together with the

117   aforementioned hourly observations of the NDBC buoys, as well as 3-hourly, hourly, and

118   every 10-min observations from other buoys, and obtained a RMS of 1 m/s. A more local

119   study at the US west coast by Pickett *et al.* (2003) showed a RMS of 1 m/s for the first 17

120   months of QuikSCAT, by using a subset of the NDBC buoys with hourly observations. None of

121   these studies performed additional temporal averaging. Bentamy, Croize-Fillon and Perigaud

122   (2008) published one of the first studies using the first eight months of ASCAT data together

123   with the hourly NDBC buoy observations and hourly averaged observations from the Tropical

124   Atmosphere Ocean (TAO) project. They showed a RMS range of 0.65-1.72 m/s depending on

125   which buoy array and which wind ranges are used. These results motivate a further analysis

126   to get deeper insights into the intercomparison between buoy and scatterometer

127   observations.

128

129   Generally, for all scatterometers wind speed, direction, and vector components are validated

130   against buoys on a monthly basis from 3 months after launch by the Ocean and Sea Ice

131   Satellite Application Facility (OSI SAF) at the Royal Netherlands Meteorological Institute

132   (KNMI). An approach for separately attributing the measurement errors to the different

133   sources of wind observations is the triple collocation approach by Stoffelen (1998). With this

134   approach, the errors of buoys, scatterometers and models are elaborated, as shown by a

135   variety of studies (e.g. Vogelzang et al. 2011; Lin et al. 2015; Stoffelen et al. 2017).

136

7

137   This work focuses on using the redundant, high-frequency (1-minute average) buoy

138   anemometer records together with independent scatterometer data to better understand

139   the uncertainty and sources of error in the buoy wind measurements. As a first step, data

140   from a site in the southeast Pacific were collocated with QuikSCAT and ASCAT observations.

141   The buoy data were converted to 10m-equivalent neutral wind speeds with two

142   parameterizations, COARE3.0 (Fairall et al. 2003) and the Liu and Tang (1996) version of the

143   Liu-Katsaros-Businger (LKB) parameterization (Liu, Katsaros, and Businger 1979). Generally,

144   the two independent observations show an RMS difference between Stratus and QuikSCAT,

145   as well as between Stratus and ASCAT, which is variable with time over the whole matching

146   period (Fig. 1a). The mean RMS when comparing to QuikSCAT is 0.71 m/s (10.2%) when using

147   COARE and 0.68 m/s (9.6%) when using LKB. The mean RMS when comparing with ASCAT is

148   0.72 m/s (10.2%) with COARE, and 0.70 m/s (9.6%) with the LKB parameterization. Two more

149   buoys (WHOTS and NTAS) are used in this paper, which were similarly compared with the

150   scatterometers resulting in RMS of 0.76 (0.68) m/s for WHOTS/QuikSCAT with the

151   COARE(LKB) parameterization and RMS of 0.71(0.66) m/s for WHOTS/ASCAT. For the NTAS

152   buoy we found RMS as low as 0.62(0.56) m/s, when converted with COARE(LKB) and

153   compared with QuikSCAT. For NTAS/ASCAT the RMSs are 0.60(0.57) m/s. A similar temporal

154   evolution can be seen for all buoys, but the temporal dependence of the RMS is not the focus

155   of this paper. In this paper, we focus on the systematic errors caused by flow distortion

156   around the buoy and its superstructure.

157

8

158   The bias between Stratus and QuikSCAT (Fig. 1b) exhibits appreciable variability over time,

159   but this seems to be mostly attributable to variations in the quality of the buoy data. The

160   largest negative values of the buoy-scatterometer bias occur in the first few Stratus

161   deployments, when we were using a different buoy and superstructure design (a 3-meter

162   discus buoy) than the one that is the focus here. (We exclude those deployments from the

163   analysis here.) The largest positive values on the bias occur in 2008, a time when both of the

164   primary anemometers had failed on the Stratus buoy. (The time series was patched with data

165   from a third, backup anemometer, but the data from this deployment were not included in

166   the flow-distortion analysis here.)   Aside from those two periods, the mean buoy-

167   scatterometer disagreement appears to be stable over time. Comparisons for the other

168   buoys were similarly stable.

169

170   This paper is organized as follows. In section 2, the buoy sites, data, and methods are

171   presented, followed by the flow distortion analysis and the comparisons between buoy and

172   scatterometer estimates in section 3. Discussion and conclusions are given in section 4.

173

174   **2. Data and methods**

175   **a) Buoy sites**

176   The WHOI UOP Group currently operates three Ocean Reference Stations (ORS): Stratus off

177   northern Chile in the eastern South Pacific, the Northwest Tropical Atlantic Station (NTAS) in

178   the northern Tropical Atlantic, and, coordinated with the Hawaii Ocean Timeseries (HOT)

179   project, the WHOI HOT Station (WHOTS) north of Oahu, Hawaii. Each ORS is maintained over

9

180   many years by successive recovery of the deployed mooring and replacement with a

181   refurbished mooring. Mooring replacements are nominally at one-year intervals. In addition

182   to the ORS, two buoys were deployed for 15 and 12 months as part of the Salinity Processes

183   in the Upper Ocean Regional Study (SPURS) project (Fig. 2; details to all buoys in Tab. 1). The

184   surface moorings are anchored to the seafloor, but the scope of the mooring allows the buoy

185   to move within 7 km of its anchor position under the influence of currents and the wind

186   around the anchor location. Buoy positions are tracked using GPS or other satellite systems.

187

188   Stratus is moored in the eastern tropical Pacific 1,100 km of the coast of Chile, in a region

189   characterized by a persistent stratus cloud deck, for the purposes of observing and

190   understanding regional air-sea interactions, providing independent surface and ocean

191   observations to motivate improvements to ocean, atmospheric, and coupled models and

192   calibrating, and validating meteorological, air-sea flux, and ocean products derived from

193   models, remote sensing methods or combinations of models and remote sensing (Colbo and

194   Weller 2007; Weller 2015).

195

196   NTAS is moored in a region of the tropical Atlantic with strong SST anomalies and the

197   likelihood of significant local air-sea interaction. The primary science objectives of the NTAS

198   project are to determine the in-situ fluxes of heat, moisture and momentum, and then to use

199   these in-situ fluxes to make a regional assessment of flux components from numerical

200   weather prediction models and satellites.

201

202   The goal of WHOTS is to provide long-term, high-quality air-sea fluxes as a coordinated part

203   of the HOT program, and contribute to the HOT goals of observing heat, momentum, fresh

204   water and chemical fluxes at a site representative of the oligotrophic North Pacific Ocean.

205

206   The first SPURS deployment was in the salinity maximum region in the subtropical North

207   Atlantic (Farrar et al. 2015), while the second SPURS deployment was in the low surface

208   salinity belt in the eastern tropical Pacific, related to the heavy rainfall within the ITCZ (Farrar

209   and Plueddemann 2019).

210

211   **b) Buoy instrumentation and physical configuration**

212   All the aforementioned buoys are fully-instrumented with either two Improved Meteorology

213   (IMET) or two Air-sea Interaction Meteorology (ASIMET) packages consisting of a suite of

214   sensors each packaged together with their signal conditioning electronics and referred to as

215   'modules' connected to power and to a data logger and satellite data telemetry system. The

216   sensor suite usually includes a module for relative humidity and air temperature (Rotronic

217   MP-101A), a barometric pressure module (Heise DXD), a precipitation module (RM Young

218   50202), a module for shortwave radiation (Eppley Precision Spectral Pyranometer), a module

219   for longwave radiation (Eppley Precision Infrared Radiometer), and a module for wind speed

220   and direction, which can be either a RM Young propeller and vane anemometer (model 5103)

221   or a Gill Sonic anemometer. To obtain the sea surface temperature (SST) a Seabird model

222   SBE37 mounted at about 1 m depth below the buoy is used. In most deployments, a third

223   anemometer, a stand-alone sensor self-contained with battery power and data logging, has

11

224   been deployed.

225

226   All the modules are mounted at different locations on the buoy (Fig. 3). The modules for air

227   temperature, humidity, barometric pressure, and the rain gauges are mounted on the

228   forward face of the upper frame. Placement of these sensors is aimed at positioning them in

229   air flow that is as undisturbed as possible, while not positioning them outboard of a tubular

230   'crash bar' that protects the tower and its sensors from encounters with the ship's hull during

231   deployment and recovery. In part, as mentioned earlier, the attempt to position them in

232   undisturbed air is accomplished by the vane that steers the buoy with respect to the wind.

233   The radiation modules are mounted as high as possible to avoid any shadows or obstructions

234   in their field of view. The SST and current sensors are mounted below the water line on the

235   buoy bridle. The two wind modules attached to the ASIMET loggers are mounted on opposite

236   sides on the forward face, opposite the buoy vane, to avoid as much flow distortion as

237   possible. We will use the terms 'port' and starboard' to distinguish between the two wind

238   modules, defining the buoy reference frame in analogy to a ship. The buoy's wind vane is on

239   the 'stern' and the opposite side of the buoy, where the anemometers are mounted, is the

240   'bow'. When looking from the stern to the bow, the buoy's port side is to the left and the

241   buoy's starboard side is to the right.

242

243   When a RM Young vane/propeller module is used for wind observations, the wind is

244   measured in five seconds (5s) segments, collecting total propeller rotations over the 5s, one

245   vane measurement each second, and a single snapshot of the compass value during these 5s.

12

246   For each 5s segment, a vector average is formed from the 5s average vane and single

247   snapshot compass. Eleven of these 5s segments are vector-averaged at the end of the one-

248   minute interval to form the final vector velocity output. A one-minute scalar average of wind

249   speed is also computed from the rotations of the propellers. After every minute the following

250   variables are stored: the vector sum of 5s velocities, the scalar averaged wind speed, the

251   maximum of the (5s) wind speeds, the last vane direction, and the last compass direction.

252

253   When a sonic anemometer is used, the following sampling scheme is applied: Each

254   measurement takes 25ms, so the base sampling rate is 40Hz. There is overhead involved to

255   output the data at the end of a sampling burst, resulting in 195 samples in a 5s interval (39

256   Hz). Within each 5s interval the compass is polled once, near the center of the interval. One-

257   minute averages are computed from 11 5s intervals with 5s of overhead for vector averaging.

258   At the end of every minute the following variables are stored: wind vector, scalar averaged

259   wind, maximum 5s wind speed, minimum 5s wind speed, last XY direction, last compass

260   direction, x-axis tilt, and y-axis tilt (where X and Y are axes in the instrument frame of

261   reference).

262

263   **c) Buoy data**

264   The data from the redundant instruments on the buoys are quality controlled to eventually

265   provide one best-estimate dataset. For the ORS, where sequential one-year deployments of

266   surface moorings have been made to collect ongoing, long-term time series, the typical

267   approach is to deploy a new surface mooring in the vicinity of the existing mooring and collect

13

268   one or more overlapping days of data. At the same time surface meteorological data are

269   collected from the ship used to service the mooring and, whenever possible, one or more

270   days of comparisons between the shipboard surface meteorology and the buoy observations

271   are made with the ship stationed downwind of the buoy, bow into the wind. This results, for

272   each deployment, in overlapping buoy data (old and new) and shipboard data. The sensors

273   on the freshly deployed buoy were calibrated before the buoy was built, and the assembled

274   buoy was run as a system both at WHOI and in port just prior to loading on the ship. These

275   "burn-in" data were scrutinized and used to identify and correct any initial problems in sensor

276   performance. After recovery, the sensors were returned for post deployment calibration.

277

278   The one-minute data from the recovered buoy were collected together with hourly averaged

279   telemetered data from the new buoy (access to the one-minute data is possible only by

280   downloading from the data logger), the shipboard data, and data from the ECMWF (European

281   Centre for Medium Range Weather Forecasts) operational model at grid points near the buoy.

282   The overlapping buoy and ship data were examined to guide correction of any drifts in the

283   recovered buoy data and the selection of the 'best' time series. For many studies the goal is

284   to create one high-quality, full-length record from the redundant sensors. Therefore, for both

285   the ORS and the SPURS deployments, post-processing developed the best corrected time

286   series from both of the buoy systems as well as the best single, complete surface

287   meteorological data set. A detailed description about data evaluation and post-processing is

288   given in Bigorre and Galbraith (2018).

289

14

290   For this study, we take advantage of the redundant sensors and the raw data of the wind

291   vector, compass, and vane were used as well as the one-minute vector-averaged winds, and

292   both the port and starboard wind records were employed. Air humidity and temperature,

293   SST, and the ocean currents were also used. Ocean currents come from the shallowest useful

294   data from a current meter deployed on the mooring line, allowing absolute and relative (i.e.

295   relative to the currents) wind speeds to be estimated for the port and the starboard sensors.

296   Furthermore, the absolute wind direction and the wind direction relative to the buoy heading

297   can be estimated. The wind module vane angle is measured relative to the buoy heading, and

298   the wind module compass measures the buoy heading—the sum of these gives the absolute

299   wind direction. To examine the flow distortion, relative differences are calculated. The

300   difference of the wind speed of the two sensors is normalized by the wind speed by one of

301   the two sensors itself to estimate the percentage difference. Because the errors are a small

302   fraction of the total wind speed, either sensor can be the divisor. Raw data for wind

303   observations (wind vector, scalar wind, vane, compass) that were obviously spurious were

304   discarded manually when they met any of the following criteria: wind vector components or

305   scalar wind speeds exactly zero, vane and compass directions higher than 400°, and vane and

306   compass directions lower than -10°. While wind observations of exactly 0 m/s are extremely

307   unlikely, vane and compass observations are only reasonable between 0 and 360°. These

308   quality-controlled data were further used either directly for intercomparison or converted to

309   equivalent neutral winds.

310

311   To compare the wind with satellite estimates, equivalent neutral wind speeds were

312   computed using two parameterizations as described above. The main reason for considering

313   LKB here is that it is still the standard parameterization for the calculation of wind data from

314   scatterometer estimates. Both parameterizations require the same data: wind components,

315   air temperature, and air humidity with its respective measurement heights; SST, and surface

316   current components. However, the COARE parameterization can utilize additional inputs

317   (barometric pressure and net solar and infrared radiation) to e.g. estimate the ocean skin

318   temperature. After several iterations a final roughness length and friction velocity is

319   estimated. With these the turbulent fluxes; transfer coefficients for momentum, latent heat,

320   and sensible heat; and the equivalent neutral wind can be calculated.

321

322   d) **Scatterometer data**

323   Two datasets of scatterometer observations are used in this study, both provided by Remote

324   Sensing Systems (RSS). The first one is from the SeaWinds scatterometer on the QuikSCAT

325   satellite ('QuikSCAT' is used to refer to the scatterometer here). QuikSCAT is a scanning

326   pencil-beam scatterometer, which was spinning from 19 July 1999 through 19 Nov 2009. We

327   used the daily gridded data files on a 0.25° longitude by 0.25° latitude grid (Ricciardulli,

328   Wentz, and Smith 2011). Rain-flagged data were discarded. Two observations per day (one

329   on an ascending and one on a descending swath) are possible and due to the sun-synchronous

330   orbit the local equator crossing time is nearly constant at 6 am for the ascending node and 6

331   pm for the descending node. To get equivalent neutral winds they used their current GMF:

332   'QuikSCAT Ku-2011' (Ricciardulli and Wentz 2015). Note, that there are other Ku-band GMFs

16

333   from other data providers. Wang et al. (2017) recently presented a new GMF for Ku-band,

334   which corrects for SSTs, named NSCAT-5. Another GMF, which accounts for SSTs, is used for

335   RapidSCAT, a scatterometer mounted on the International Space Station (ISS). This GMF is

336   called KuSST and is an extension of the Ku-2011 GMF mentioned before.

337

338   The second scatterometer data product is ASCAT-A, also obtained from RSS. Note, there are

339   several different products with different quality using the same original data (see e.g., Wang

340   et al. 2019). ASCAT is a scatterometer onboard the MetOp-A satellite and operating in C-band.

341   The first data are available from 1 March 2007 and it is still operating. As for QuikSCAT we

342   used the daily data files on a 0.25° longitude by 0.25° latitude grid (Ricciardulli and Wentz

343   2016) and discarded rain-flagged data. Again, two observations per day are possible and the

344   sun-synchronous orbit has nearly constant equator crossing times at 9:30 am for the

345   ascending node and 9:30 pm for the descending node. ASCAT-A is very stable over time at

346   the three aforementioned ORS buoy sites (cf. Fig 1b for Stratus).

347

348   **e) Methods**

349   A common issue in comparing two observations, which have different time and space

350   resolution, is their collocation. Each of the 14 daily orbits around the globe is covered in about

351   90 minutes, in which a large area is observed in a short time. The gridded product which is

352   used provides a time in minutes as well. The smallest time increment is about six minutes.

353   The task is to match these satellite data to the buoy observation, which is within its watch

354   circle (~7 km) and has data on the resolution of one minute. The satellite is matched to the

17

355   nearest minute in time of the buoy time series and the closest grid point is used. Furthermore,

356   the buoy data are averaged with a running mean over a specific time, as discussed below. The

357   spatial representation can introduce a bias when comparing averaged wind vectors over a

358   large area with local wind vectors.

359

360   The RMS between satellite and buoy wind speeds shows a dependence on the averaging time,

361   regardless of which scatterometer or buoy is used (Fig. 4). All possible averaging times

362   between one minute (i.e. original resolution) and 400 minutes were used, subdivided in one-

363   minute increments. Assuming a mean wind of 7 m/s, which is approximately the case for all

364   considered buoy sites, this wind covers approximately 25 km in an hour, which is the size of

365   a region related to one grid point. However, the dynamic range of the wind is between wind

366   speeds close to 0 m/s up to almost 20 m/s. Therefore, the averaging distance is not constant

367   for a single averaging time. To account for this, we used the approach of Lin *et al.* (2015) to

368   estimate 25-km equivalent buoy winds. Specifically, for a scatterometer grid cell of $\Delta x = 25$

369   km, we chose an averaging interval of $\Delta t = \Delta x / U$ where U is the wind vector average around

370   the time of the satellite overpass with one-minute resolution and Δt is the sum of the time in

371   one-minute increments. The summation is done until Δx reaches 25 km. The resulting

372   averaging periods (Δt) range between 30 minutes and seven hours. We denote each averaged

373   result a "buoy match" and those winds are used in this paper whenever a comparison

374   between satellite and buoy data is shown.

375

18

376   We finally have time series of buoy observations of the wind vector from each sensor, the

377   converted equivalent neutral wind speeds from each sensor (converted in the described way,

378   not considering air mass density effects), and a time series of buoy matches, again separately

379   for each sensor.

380

381   With the time series of buoy matches and scatterometer observations, RMS differences were

382   computed. A period of 48 scatterometer-buoy-matches was used for that, i.e. 48 is the size

383   of the window used for the RMS computation and represents 24.2 days on average (cf. e.g.

384   Fig. 1a). RMSs are provided either by the actual value in units of wind speed (m/s) or relative

385   (%). The relative RMS is the quotient of the RMS and the averaged buoy wind speed over the

386   considered period, multiplied by 100%.

387

388   **3. Flow distortion**

389   The first part of this section is about the flow distortion around the buoys with a few

390   examples. The flow distortion at the buoy is investigated using the two wind observations at

391   different positions on the buoy, port and starboard. The two sensors observe different wind

392   speeds, while the true wind speed is not known.

393

394   The results of the CFD study (Emond et al. 2012) mentioned earlier will be introduced first.

395   The study used a model mesh of the buoy which is comparable to the real buoys used in the

396   ocean. The big advantage of a model study is, that the 'true' wind is known and the 'observed'

397   wind at any arbitrary position on the model mesh can be compared to it. The tendency of the

19

398   buoy to remain in a constant angle of about 30° relative to the flow for long times was

399   accounted for the CFD study. When the buoy's bow is oriented at 30° to the incident wind,

400   the simulations showed a systematic positive wind speed bias at the downstream wind sensor

401   of about 3.5% and a negative bias at the upstream sensor of about 1% (Fig. 5). We will return

402   to these results later when examining the buoy-scatterometer disagreements.

403

404   Using now the real buoy observations, first we present an example from the seventh

405   deployment of the Stratus buoy. The time series of hourly averages of relative wind speeds

406   of the two sensors agree quite well, indicating the general good performance of both sensors

407   (Fig. 6a). The difference between them is generally below 0.3 m/s for the whole deployment

408   period of more than one year (Fig. 6b). The absolute wind direction indicates a nearly

409   constant regime of southeasterly winds, which are the trade winds in this part of the

410   subtropical southeast Pacific (Fig. 6c). The wind directions of the two sensors are not the

411   same. A dominant bias of around 10° is clearly visible, showing that the port sensor mostly

412   observed more southerly wind directions (Fig. 6d). Changes in this difference usually

413   occurred, when low wind speeds of less than 5 m/s were observed. These changes came along

414   with changes or even jumps in the wind direction of both sensors. However, directional errors

415   are not considered in this analysis.

416

417   Calculating the relative difference of wind speeds of the two sensors, a dependence on the

418   wind direction relative to the buoy is obvious (Fig. 7). Generally, the buoy tends to move in

419   both directions relative to the wind direction. This results from the interaction of either the

20

420   buoy vane, which tries to align the buoy in the wind, and a torque, which follows from the

421   wind action at the buoy storage well and the superstructure (Emond et al. 2012). Within a

422   deviation of 50° to either side from the direction aligned with the buoy vane (0°), a linear

423   relation can be observed. The relative difference is positive, when subtracting the near-side

424   observation from the far side, i.e. when the wind blows from port direction (negative abscissa

425   in Fig. 7) the difference of the starboard minus the port observation is positive. This linear

426   dependence is valid for more than 80% of all deployments, regardless of the investigated

427   buoy.

428

429   The seventh deployment of Stratus was chosen because it represents a "clean" example of a

430   linear relation. The slope of the linear relation, the offset in the wind difference (i.e. the

431   crossing of the y-axis), the maximum bias, as well as the spread of the deviation of the buoy

432   orientation from the relative north are different for each deployment. Generally, the range

433   of the bias is about 5%, though can be up to 10% for a few deployments, but also can be

434   smaller than 5% too. The range of angles, from which the wind impinges at the buoy, can

435   differ from a couple of degrees to almost the full circle (180° from either side). Relative wind

436   directions greater than 50° from one side are generally susceptible to additional errors,

437   because the flow toward the far sensor can be significantly more distorted by the buoy

438   superstructure or the upstream sensor itself. After several deployments the vane design was

439   changed to a larger one and in the following deployments relative directions larger than 50°

440   in either direction were rare, leading to a more stable position around the buoy north.

441

21

442   The satellite datasets from QuikSCAT and ASCAT are useful for getting insight into the

443   disagreement between the two buoy anemometers. For the comparison with satellite

444   observations, the buoy wind speeds were converted into equivalent neutral wind speeds. To

445   increase the amount of data, several deployments, at which the flow distortion behavior is

446   similar, were analyzed together. Nevertheless, only deployments where the offset was close

447   to zero, i.e. the wind speed difference was zero at relative directions close to zero, were used.

448   Slightly less than half (22 out of 45) of all deployments met these conditions (cf. furthermost

449   right column of Tab. 1). The remaining deployments show either no linear structure at all,

450   which is mostly related to failure of one wind module, or they show a similar linear behavior

451   between the two wind measurements, but exhibit some additional offset. At those

452   deployments some additional source of uncertainty has an influence.

453

454   First, the Stratus deployments 4, 5, 6, and 7 were merged with the NTAS deployments 2, 4, 5,

455   6, and 8. These nine deployments are from a period when QuikSCAT was providing wind data

456   and altogether consist of 4446 satellite-buoy matchups. This subsample of the buoy data can

457   be plotted as a function of the wind incidence angle relative to the buoy in the same way as

458   described before. A similar structure in the relative difference of the equivalent neutral wind

459   speeds for all data is common. Using only the data of the matches with the QuikSCAT passes,

460   the linear relation remains the same (Fig. 8a) for the wind directions between the buoy north

461   and 50° from either side. This means that the subsample of the buoy data that is co-located

462   with the satellite data is a good representation of the whole dataset. The probability

22

463   distribution of the data shows a maximum close to the zero wind direction, slightly deviated

464   to starboard winds, with small differences between the two modules (Fig. 8b).

465

466   Similar to the QuikSCAT period, the same was done for the ASCAT period. Here, the Stratus

467   deployments 7, 11, 13, and 15 were merged with the NTAS deployments 8, 10, and 11, the

468   WHOTS deployments 4, 5, 7, 10, 11, 12, and 13, and the first SPURS deployment. This led to

469   3832 matchups. The final figure with all ASCAT-matching data points again shows the linear

470   relation (Fig. 8c). The probability distribution shows a symmetric structure with most of the

471   data around zero relative wind direction (Fig. 8d). Both QuikSCAT and ASCAT results are

472   consistent with the CFD flow simulations and suggest a systematic error induced by the flow

473   distortion around the buoy. This is true for all applicable data sets of redundant buoy

474   observations, either the whole time series or the subset of scatterometer matches.

475

476   The CFD simulations predicted an asymmetric effect of flow distortion, with the upwind

477   sensor having a negative wind speed bias that is slightly smaller than the positive wind speed

478   bias on the downwind sensor. However, this asymmetry in the errors cannot be detected

479   when examining the difference between the two sensors, because the differencing

480   operations effectively combines the bias of the two sensors into a single number. Replacing

481   one of the sensors with QuikSCAT or ASCAT observations enables us to possibly indicate the

482   effect of the flow distortion. When plotted as a function of wind incidence angle in the buoy

483   reference frame, the bin-averaged RMS difference between the buoy and scatterometer

484   wind speeds resembles the comparison of port-starboard buoy anemometers (grey stars in

23

485   Fig. 9). However, the linear relation between incidence angle and RMS disagreement is offset

486   in the way that the average of the considered scatterometer data is always higher than the

487   buoy average. This bias is about 1.1%, regardless which scatterometer product is used and

488   compared to all considered buoy data. Taking the overall mean wind speed estimates from

489   the scatterometers into account (QSCAT: 7.3 m/s; ASCAT: 7.5 m/s), the absolute bias is about

490   0.08 m/s. This small bias could have many reasons, like atmospheric conditions, waves, or an

491   additional effect of flow distortion. Note, that the calibration of scatterometers against buoys

492   to get a bias close to zero is done at the global average level. Somewhat arbitrarily, the offset

493   was subtracted from the satellite time series (blue stars in Fig. 9). For incidence angles within

494   ±40°, the buoy-scatterometer differences are in good agreement with the CFD prediction by

495   Emond *et al.* (2012)—the upwind sensor has a negative wind speed bias that is slightly lower

496   than the positive bias seen on the downwind sensor (compare to red crosses in Fig. 9).

497

498   Three lines of evidence-- from the CFD simulations, from the port-starboard anemometer

499   comparison, and from the scatterometer-buoy comparison-- support the conclusion that

500   there are flow distortion errors in the buoy wind speeds. Because these wind speed errors

501   seem to be a systematic function of the buoy incidence angle, we explored the possibility of

502   making a correction to remove the flow distortion error from the module time series. Two

503   attempts were made with the original time series of the two modules. The first approach was

504   the application of the theoretical error between the two modules for the deviation of 30° on

505   either side, as predicted by the CFD study. Emond *et al.* (2012) showed a relative error of

506   +3.44% on the downwind side, and -1.03% on the upwind side. Applying this correction by

24

507   linearly interpolating between -30° and 30° (the two largest angles used in Emond *et al.*, 2012)

508   shows significant improvement in terms of the dependency of the module differences to the

509   wind direction (red stars in Fig 10). The second approach was using the same CFD prediction,

510   but applying the results to the observed error. This was done by using the error proportion

511   at -30° and 30° from the CFD study (3.44% to -1.03%) to partition the port-starboard

512   anemometer difference between the two anemometers. In the CFD study, the upwind

513   anemometer was 1.03% low and the downwind anemometer was 3.44% high, so 23% of the

514   inter-anemometer disagreement should be attributed to a low bias in the upwind

515   anemometer and 77% should be attributed to a high bias in the downwind anemometer. This

516   relation was then interpolated between -30 and 30° and applied to the observed error for

517   every wind direction. The second correction appears to almost perfectly remove the flow

518   distortion errors from the module time series (green stars in Fig. 10), but this is by

519   construction because the mean inter-anemometer disagreement at each angle is necessarily

520   zero after application of this correction.

521

4. Discussion and conclusions

523   Wind observations from moored buoys were used in this study. Generally, those

524   measurements are taken at about 3m height on a platform (the buoy) that is moving in

525   response to the wind, the waves, and the currents. Although wind measurements have been

526   collected from buoys for many decades now, careful analysis is still needed to estimate and

527   minimize the influence of errors.

528

529   **a) Flow distortion**

530   Flow distortion is one of these error sources. The influence of flow distortion was examined

531   using different WHOI buoys, and the relative disagreement of redundant anemometer wind

532   speeds on the buoy reaches 5%, with a systematic dependence on the incidence angle of the

533   wind relative to the buoy. For incidence angles within 50° of the buoy's bow, a linear relation

534   is identified. This is valid for more than 80% of all deployments. Using half of the deployments

535   (22 out of 45) that showed an inter-anemometer disagreement deemed "typical", the effect

536   of flow distortion on the error could be estimated. This incidence-angle dependence is

537   supported through comparison to measurements from scatterometers. We applied a

538   correction for the flow distortion in the comparison between scatterometers and buoys. The

539   dependence on the incidence angle almost disappears when the aforementioned bias of 1.1%

540   and either of two flow distortion corrections based on the CFD simulations are applied (Fig.

541   11).

542

543   We are not aware of many published studies of flow distortion in wind measurements from

544   oceanographic buoys. Similar results were estimated by Bigorre *et al.* (2013), using a much

545   smaller data set from the same type of buoy deployed in the Gulf Stream region. A CFD study

546   has shown that the "faster" side of the buoy is high biased and the absolute value of this high

547   bias is larger than the absolute value of the low bias on the "slower" side where the wind is

548   coming from (Emond et al. 2012). The CFD simulations are certainly illuminating, but they

549   were done for an idealized setting, with no wave motion or tilt on the buoy, and so we sought

26

550   to also use independent data sets from QuikSCAT and ASCAT-A to try to assess the buoy

551   errors.

552

553   All these results give an important overview over the systematic errors related to flow

554   distortion and the necessity to take them into account when using buoy observations as part

555   of a ground truth for calibration and validation of satellite based wind estimates.

556

557   **b) Other error sources**

558   It was also shown that the RMS between the equivalent neutral winds estimated from buoy

559   observations and satellite measurements is as low as half a meter per second. Several

560   additional aspects have to be considered when comparing direct wind observations on buoys

561   with satellite-based estimates of near-surface winds:

562

563   i. **Currents**

564   The scatterometer observes the sea surface, on which both the wind and the ocean itself act.

565   Therefore, the scatterometer observes a wind relative to the surface currents. To compare

566   them with buoy observations, the buoy wind has to be corrected for the currents to get

567   relative winds. We used relative winds in this study, because all considered buoy

568   deployments also observe the near-surface currents. Therefore, the impact of surface

569   currents on the error is expected to be negligible in this study.

570

571   ii. **Collocation and averaging**

27

572   One of the big issues is the collocation of the different independent data in space and time.

573   Spatial and temporal representation errors are introduced by comparing averaged wind

574   vectors over a large area (here 25km) with local wind vectors. Stoffelen (1998) showed with

575   a triple collocation approach, that the NOAA buoys have the largest error variance compared

576   with scatterometers and a NCEP forecast model. May and Bourassa (2011) showed a nice

577   approach of assessing the uncertainty between shipboard in-situ data and scatterometer

578   estimates. They deduced, that the main contribution to the total variance of the differences

579   of collocated ship and scatterometer observations depends on the temporal difference

580   between them. For differences less than 25 min only the variances of the datasets itself need

581   to be considered, while the variance related to temporal and spatial differences needs to be

582   accounted for differences greater than 25 min. This temporal difference between in-situ and

583   scatterometer observation is important for buoys also. We took advantage of the 1-minute

584   temporal resolution of the buoy data and compared in this study two approaches of

585   collocating the different data types. One is the fixed-time averaging of the buoy time series,

586   which would lead to one-hour averaging. The second approach is a variable averaging period

587   described by Lin *et al.* (2015). The wind speed is converted into a corresponding distance; this

588   distance is added together over time until it reaches an equivalent of 25 km. The differences

589   between the two approaches are small. The RMS differences with the second approach are

590   slightly smaller, though, and eventually, the second approach was used. The spatiotemporal

591   averaging of buoy and scatterometer is expected to be much more important when

592   comparing scatterometers to buoys that do not have the 1-minute temporal resolution that

593   is available on WHOI buoys. For buoys with less temporal resolution, a collocation window of

594   up to 30 min between buoy and scatterometer might still provide good estimates of buoy-

595   scatterometer uncertainty.

596

597   **iii.   Viscosity**

598   A correction due to misrepresented viscosity, related to SSTs, was investigated following

599   Bentamy *et al.* (2012) (not shown). In a recent paper, Wang et al. (2017) showed the

600   dependence of the SST effect on radar frequency, polarization and the incidence angle. The

601   temporal variations in water viscosity are important for scatterometers because this affects

602   the wave behavior at the centimeter scales that dominate the radar backscatter. This only

603   marginally reduces the RMS. While the viscosity is directly related to the SST, the effect of

604   the viscosity is seasonally varying and can explain a portion of the variability in the RMS

605   between buoys and scatterometers (cf. Fig. 1). However, this effect is only relevant in very

606   cold waters and the viscosity correction was not applied to the scatterometer data.

607

608   **iv.   GMF and scatterometer errors**

609   The GMFs for Ku-band are also SST dependent (see e.g., Wang et al. 2017), which is neglected

610   in the Ku-2011 GMF used here. The SST varies at the Stratus site seasonally between 18 and

611   23 °C, at NTAS between 25 and 29 °C, and at WHOTS between 23 and 28 °C. Furthermore, the

612   Ku-band GMF is not directly related to stress, because it uses equivalent neutral winds at 10m

613   height. It misses the atmospheric mass density, mainly related to humidity (De Kloe et al.

614   2017). Following them, the air mass density varies between 1.16 and 1.22 kg/m3, yielding to

615   wind speed differences (u10s-u10n) between 0 and -0.2 m/s. Therefore, the consideration of

29

616   atmospheric mass density decreases the equivalent neutral wind speed in 10m up to 0.2 m/s

617   (seasonally varying).

618

619   Scatterometers itself exhibit some temporal variability in terms of their speeds, wind

620   component statistics and their differences with respect to buoys and models (see e.g.,

621   Verhoef et al. 2017). However, the scatterometers used in this study are temporally stable

622   over the considered time period.

623

624   **v.   Seasonal cycles**

625   Related to the aforementioned variability, seasonal cycles in the RMS are present as well (not

626   shown). The seasonal cycle is similar at each buoy, but can differ strongly between sites. The

627   seasonal cycles most likely result from other parameters and their seasonal evolution as

628   described before. Unresolved gustiness is another possible source of seasonality. It was

629   shown that scatterometers by themselves also observe a seasonality related to enhanced

630   wind variability in the summer hemisphere (Belmonte Rivas et al. 2017). Moist convection

631   can be one of the reasons for this. The temporal cycles of RMS differences are beyond the

632   scope of this paper, but may be appropriate for a separate study.

633

634   Most of the time the RMS is about 0.56-0.76 m/s. The mentioned studies explain much of the

635   differences between scatterometer and buoy observations of winds. Furthermore, Lin et al.

636   (2015) deduced that the comparison of buoys and scatterometers is largely determined by

637   buoy location, data screening and season. Generally, in-situ observations on buoys and

638   scatterometers, both different kinds of wind observations, show a consistent behavior over

639   periods already longer than a decade. Therefore, both are very reliable by themselves. This

640   highlights the continued importance of in-situ point measurements from buoys for the

641   purpose of scatterometer calibration. Furthermore, they can be used to validate gridded wind

642   products. On the other hand, calibrated scatterometers can be used for spatial and temporal

643   validation of reanalysis winds, as shown by e.g. Belmonte Rivas and Stoffelen (2019).

644

645   **c) Conclusion**

646   The influence of flow distortion was examined using different WHOI buoys together with

647   scatterometer measurements. The relative disagreement of redundant anemometer wind

648   speeds on the buoy can be up to 5% of the wind speed, with a systematic dependence on the

649   incidence angle of the wind relative to the buoy. This is in agreement with expectations based

650   on simulations of the flow distortion around the buoy superstructures. The flow distortion

651   errors can be corrected to some extent.

652

653

654   We have focused on the measurement errors in buoy winds, errors that exist despite efforts

655   made by many people over several decades to identify and eliminate them. Scatterometers

656   also have issues and biases that have also been the focus of sustained research and

657   engineering efforts. Measurement errors from these instruments can be subtle and can

658   change with time, and it is only by careful intercomparisons of independent measurements

31

659   that we can be confident that we know the wind. A robust observing system for winds needs

660   to include both buoys and scatterometers.

661   **Acknowledgments**

678

679   **References**

680   Belmonte Rivas, Maria, and Ad Stoffelen. 2019. "Characterizing ERA-Interim and ERA5 Surface

32

681   Wind Biases Using ASCAT." *Ocean Science* 15 (3): 831–52. https://doi.org/10.5194/os-15-

682   831-2019.

683 Belmonte Rivas, Maria, Ad Stoffelen, Jeroen Verspeek, Anton Verhoef, Xavier Neyt, and Craig

684   Anderson. 2017. "Cone Metrics: A New Tool for the Intercomparison of Scatterometer

685   Records." *IEEE Journal of Selected Topics in Applied Earth Observations and Remote*

686   *Sensing* 10 (5): 2195–2204.

687 Bentamy, Abderrahim, Denis Croize-Fillon, and C Perigaud. 2008. "Characterization of ASCAT

688   Measurements Based on Buoy and QuikSCAT Wind Vector Observations." *Ocean Science* 4

689   (4): 265–74.

690 Bentamy, Abderrahim, Semyon A. Grodsky, James A. Carton, Denis Croizé-Fillon, and Bertrand

691   Chapron. 2012. "Matching ASCAT and QuikSCAT Winds." *Journal of Geophysical Research:*

692   *Oceans* 117 (2): 1–15. https://doi.org/10.1029/2011JC007479.

693 Bigorre, Sébastien P., Robert A. Weller, James B. Edson, and Jonathan D. Ware. 2013. "A Surface

694   Mooring for Air-Sea Interaction Research in the Gulf Stream. Part II: Analysis of the

695   Observations and Their Accuracies." *Journal of Atmospheric and Oceanic Technology* 30

696   (3): 450–69. https://doi.org/10.1175/JTECH-D-12-00078.1.

697 Bigorre, Sébastien P, and Nancy R Galbraith. 2018. "Sensor Performance and Data Quality

698   Control." In *Observing the Oceans in Real Time*, edited by R Venkatesan, Amit Tandon, Eric

699   D'Asaro, and M A Atmanand, 243–61. Cham: Springer International Publishing.

700   https://doi.org/10.1007/978-3-319-66493-4_12.

701 Colbo, Keir, and Robert Weller. 2007. "The Variability and Heat Budget of the Upper Ocean

702   under the Chile-Peru Stratus," 607–37.

703   Colbo, Keir, and Robert A Weller. 2009. "Accuracy of the IMET Sensor Package in the

704   Subtropics." *Journal of Atmospheric and Oceanic Technology* 26 (9): 1867–90.

705   https://doi.org/10.1175/2009JTECHO667.1.

706   Ebuchi, Naoto, Hans C Graber, and Michael J Caruso. 2002. "Evaluation of Wind Vectors

707   Observed by QuikSCAT/SeaWinds Using Ocean Buoy Data." *Journal of Atmospheric and*

708   *Oceanic Technology* 19 (12): 2049–62. https://doi.org/10.1175/1520-

709   0426(2002)019<2049:EOWVOB>2.0.CO;2.

710   Emond, M, D Vandemark, J Forsythe, A J Plueddermann, and J T Farrar. 2012. "Flow Distortion

711   Investigation of Wind Velocity Perturbations for Two Ocean Meteorological Platforms," no.

712   WHOI-2012-02: 66. http://hdl.handle.net/1912/5182.

713   Fairall, C. W., E. F. Bradley, J. E. Hare, A. A. Grachev, and J. B. Edson. 2003. "Bulk

714   Parameterization of Air-Sea Fluxes: Updates and Verification for the COARE Algorithm."

715   *Journal of Climate* 16 (4): 571–91. https://doi.org/10.1175/1520-

716   0442(2003)016<0571:BPOASF>2.0.CO;2.

717   Farrar, J Thomas, and Albert J Plueddemann. 2019. "On the Factors Driving Upper-Ocean

718   Salinity Variability at the Western Edge of the Eastern Pacific Fresh Pool." *Oceanography* in

719   press.

720   Farrar, J Thomas, Luc Rainville, Albert J Plueddemann, William S Kessler, Craig Lee, Benjamin A

721   Hodges, Raymond W Schmitt, et al. 2015. "Salinity and Temperature Balances at the SPURS

722   Central Mooring During Fall and Winter." *Oceanography* 28 (1): 56–65.

723   http://www.jstor.org/stable/24861843.

724   Figa-Saldaña, J., J. J.W. Wilson, E. Attema, R. Gelsthorpe, M. R. Drinkwater, and A. Stoffelen.

725   2002. "The Advanced Scatterometer (Ascat) on the Meteorological Operational (MetOp)

726   Platform: A Follow on for European Wind Scatterometers." *Canadian Journal of Remote*

727   *Sensing* 28 (3): 404–12. https://doi.org/10.5589/m02-035.

728   Freilich, Michael H., and R. Scott Dunbar. 1999. "The Accuracy of the NSCAT 1 Vector Winds:

729   Comparisons with National Data Buoy Center Buoys." *Journal of Geophysical Research:*

730   *Oceans* 104 (C5): 11231–46. https://doi.org/10.1029/1998JC900091.

731   Kloe, Jos De, Ad Stoffelen, and Anton Verhoef. 2017. "Improved Use of Scatterometer

732   Measurements by Using Stress-Equivalent Reference Winds." *IEEE Journal of Selected*

733   *Topics in Applied Earth Observations and Remote Sensing* 10 (5): 2340–47.

734   https://doi.org/10.1109/JSTARS.2017.2685242.

735   Lin, Wenming, Marcos Portabella, Ad Stoffelen, Anton Verhoef, and Antonio Turiel. 2015.

736   "ASCAT Wind Quality Control Near Rain." *IEEE Transactions on Geoscience and Remote*

737   *Sensing* 53 (8): 4165–77. https://doi.org/10.1109/TGRS.2015.2392372.

738   Lin, Wenming, Marcos Portabella, Ad Stoffelen, Jur Vogelzang, and Anton Verhoef. 2015.

739   "ASCAT Wind Quality under High Subcell Wind Variability Conditions." *Journal of*

740   *Geophysical Research: Oceans* 120 (8): 5804–19. https://doi.org/10.1002/2015JC010861.

741   Liu, W Timothy, Kristina B Katsaros, and Joost A Businger. 1979. "Bulk Parameterization of Air-

742   Sea Exchanges of Heat and Water Vapor Including the Molecular Constraints at the

743   Interface." *Journal of the Atmospheric Sciences* 36 (9): 1722–35.

744   https://doi.org/10.1175/1520-0469(1979)036<1722:BPOASE>2.0.CO;2.

745   Liu, W Timothy, and Wenqing Tang. 1996. "Equivalent Neutral Wind." *JPL Publication*, 17–96.

746   Lungu, Ted, and P S Callahan. 2006. "QuikSCAT Science Data Product User's Manual: Overview

747   and Geophysical Data Products." *D-18053-Rev A, Version* 3: 91.

748   May, Jackie C., and Mark A. Bourassa. 2011. "Quantifying Variance Due to Temporal and Spatial

749   Difference between Ship and Satellite Winds." *Journal of Geophysical Research: Oceans*

750   116 (8): 1–15. https://doi.org/10.1029/2010JC006931.

751   Pickett, Mark H., Wenqing Tang, Leslie K. Rosenfeld, and Carlyle H. Wash. 2003. "QuikSCAT

752   Satellite Comparisons with Nearshore Buoy Wind Data off the U.S. West Coast." *Journal of*

753   *Atmospheric and Oceanic Technology* 20 (12): 1869–79. https://doi.org/10.1175/1520-

754   0426(2003)020<1869:QSCWNB>2.0.CO;2.

755   Ricciardulli, L., F. J. Wentz, and D. K. Smith. 2011. "Remote Sensing Systems QuikSCAT Ku-2011

756   Daily and Weekly Ocean Vector Winds on 0.25 Deg Grid, Version 4, Remote Sensing

757   Systems, Santa Rosa, CA. Available Online at Www.Remss.Com/Missions/Qscat. [Accessed

758   16 May 2018]."

759   Ricciardulli, L., and F.J. Wentz. 2016. "Remote Sensing Systems ASCAT C-2015 Daily Ocean

760   Vector Winds on 0.25 Deg Grid, Version 02.1. Santa Rosa, CA: Remote Sensing Systems.

761   Available at Www.Remss.Com/Missions/Ascat. Accessed [16 May 2018]."

762   Ricciardulli, Lucrezia, and Frank J. Wentz. 2015. "A Scatterometer Geophysical Model Function

763   for Climate-Quality Winds: QuikSCAT Ku-2011." *Journal of Atmospheric and Oceanic*

764   *Technology* 32 (10): 1829–46. https://doi.org/10.1175/JTECH-D-15-0008.1.

765   Stoffelen, Ad. 1998. "Toward the True Near-Surface Wind Speed : Error Modeling and

766   Calibration Using Triple Collocation." *Journal of Geophysical Research* 103: 7755–66.

767   Stoffelen, Ad, and Marcos Portabella. 2006. "On Bayesian Scatterometer Wind Inversion." *IEEE*

768   *Transactions on Geoscience and Remote Sensing* 44 (6): 1523–33.

769   https://doi.org/10.1109/TGRS.2005.862502.

770   Stoffelen, Ad, Jeroen Adriaan Verspeek, Jur Vogelzang, and Anton Verhoef. 2017. "The CMOD7

771   Geophysical Model Function for ASCAT and ERS Wind Retrievals." *IEEE Journal of Selected*

772   *Topics in Applied Earth Observations and Remote Sensing* 10 (2): 2123–34.

773   https://doi.org/10.1109/JSTARS.2017.2681806.

774   Verhoef, Anton, Jur Vogelzang, Jeroen Verspeek, and Ad Stoffelen. 2017. "Long-Term

775   Scatterometer Wind Climate Data Records." *IEEE Journal of Selected Topics in Applied*

776   *Earth Observations and Remote Sensing* 10 (5): 2186–94.

777   https://doi.org/10.1109/JSTARS.2016.2615873.

778   Vogelzang, Jur, Ad Stoffelen, Anton Verhoef, and Julia Figa-Saldaña. 2011. "On the Quality of

779   High-Resolution Scatterometer Winds." *Journal of Geophysical Research: Oceans* 116 (10):

780   1–14. https://doi.org/10.1029/2010JC006640.

781   Wang, Z, A Stoffelen, F Fois, A Verhoef, C Zhao, M Lin, and G Chen. 2017. "SST Dependence of

782   Ku- and C-Band Backscatter Measurements." *IEEE Journal of Selected Topics in Applied*

783   *Earth Observations and Remote Sensing* 10 (5): 2135–46.

784   https://doi.org/10.1109/JSTARS.2016.2600749.

785   Wang, Zhixiong, Ad Stoffelen, Biao Zhang, Yijun He, Wenming Lin, and Xiuzhong Li. 2019.

786   "Inconsistencies in Scatterometer Wind Products Based on ASCAT and OSCAT-2

787   Collocations." *Remote Sensing of Environment* 225 (February): 207–16.

788   https://doi.org/10.1016/j.rse.2019.03.005.

789   Wang, Zhixiong, Ad Stoffelen, Chaofang Zhao, Jur Vogelzang, Anton Verhoef, Jeroen Verspeek,

790   Mingsen Lin, and Ge Chen. 2017. "An SST-Dependent Ku-Band Geophysical Model Function

37

791   for RapidScat." *Journal of Geophysical Research: Oceans* 122: 1–22.

792   https://doi.org/10.1002/2016JC012264.Received.

793 Weissman, D. E., B. W. Stiles, S. M. Hristova-Veleva, D. G. Long, D. K. Smith, K. A. Hilburn, and

794   W. L. Jones. 2012. "Challenges to Satellite Sensors of Ocean Winds: Addressing

795   Precipitation Effects." *Journal of Atmospheric and Oceanic Technology* 29 (3): 356–74.

796   https://doi.org/10.1175/JTECH-D-11-00054.1.

797 Weller, Robert A. 2015. "Variability and Trends in Surface Meteorology and Air – Sea Fluxes at a

798   Site off Northern Chile." *Journal of Climate*, 3004–23. https://doi.org/10.1175/JCLI-D-14-

799   00591.1.

800 Yu, Lisan, and Xiangze Jin. 2012. "Buoy Perspective of a High-Resolution Global Ocean Vector

801   Wind Analysis Constructed from Passive Radiometers and Active Scatterometers (1987-

802   Present)." *Journal of Geophysical Research: Oceans* 117 (11): 1–24.

803   https://doi.org/10.1029/2012JC008069.

804

805

Tables

807   *Table 1. Overview of the buoys. Approximate locations are given. The exact location of the*

808   *anchor varies slightly from one deployment to the next.*

Buoy	Latitude	Longitude	Operation period	No. of deployments	
				All	Used for flow distort.
Stratus	20° S	85° W	10/2000-present	15	7
NTAS	15° N	51° W	03/2001-present	15	7
WHOTS	22° 45' N	158° W	08/2004-present	13	7
SPURS 1	24° 30' N	38° W	09/2012-09/2013	1	1
SPURS 2	10° N	125° W	08/2016-11/2017	1	0

809

810 **Figures**

811

812

813
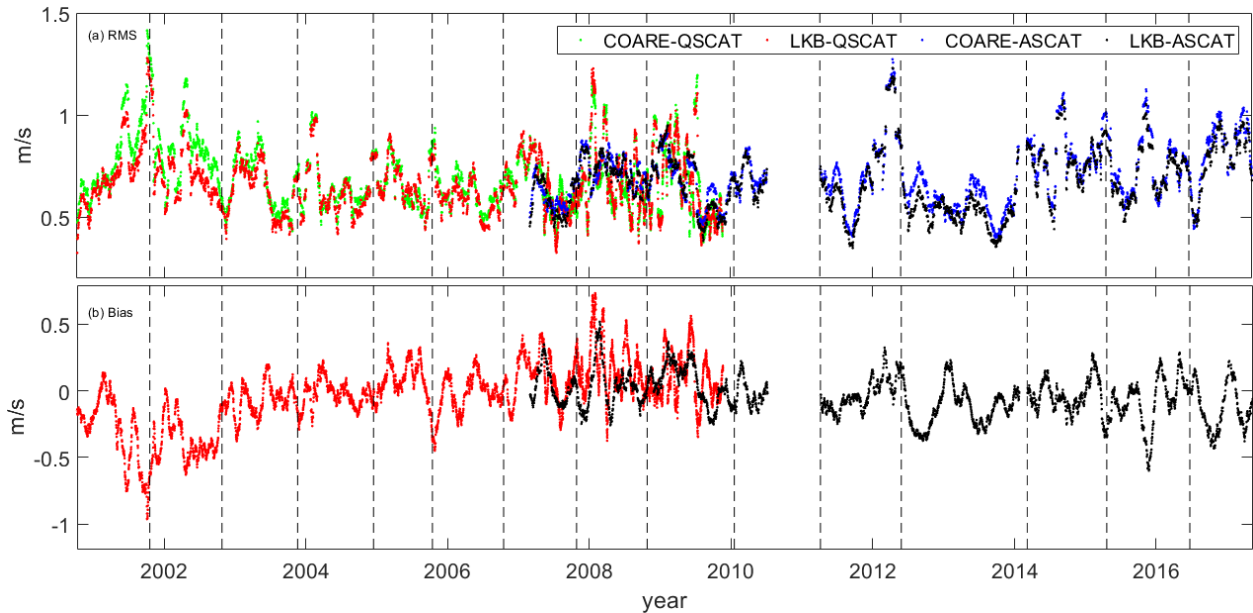
814 *Figure 1. (a) RMS difference between Stratus and QuikSCAT (red and green lines) and ASCAT*

815 *(black and blue lines). The Stratus equivalent neutral winds were estimated with the COARE*

816 *(green and blue) and LKB (red and black) parameterizations. The RMS differences were*

817 *computed over 48 consecutive matchups of buoy and scatterometer observations (cf. the last*

818 *paragraph of section 2). (b) Bias between the buoy and scatterometers for the same 48-pt*

819 *intervals (only the LKB buoy wind is shown). Note that the buoy design considered here was*

820 *used only after 2004.*

821

40

822
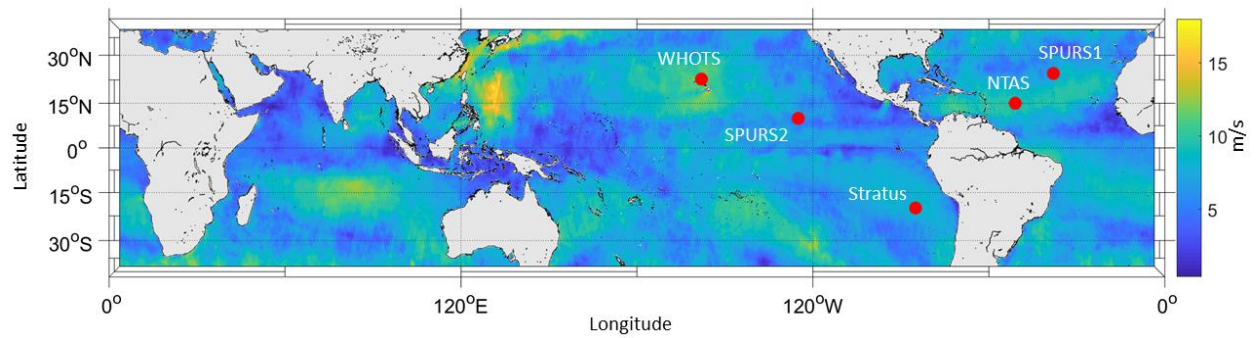
Figure 2. Mean wind speed in the global tropical and subtropical ocean as seen from ASCAT on

October 21 2017. The red dots show the sites of the three Ocean Reference Stations (WHOTS,

NTAS, and Stratus) and the two SPURS sites.

41
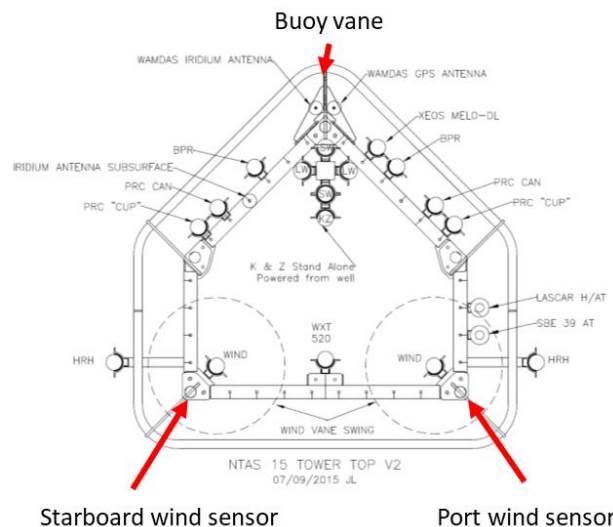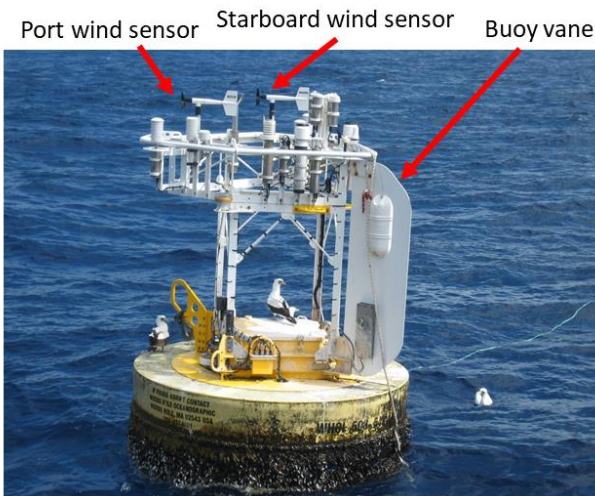
826

827 *Figure 3. The Stratus buoy before recovery from its 13th deployment (left), and the NTAS buoy*

828 *schematic for its 15th deployment (top view; right). Aluminum tubing forms an outer protective*

829 *perimeter or "crash bar" to absorb contacts the ship's hull. Two humidity/temperature sensors*

830 *(HRH) are outboard of the crash bar but the anemometers are inboard on the forward face, with*

831 *the arc the swing of the anemometers' vanes inside the crash bar. In the center of the buoy is*

832 *the storage well housing batteries and electronics.*

833
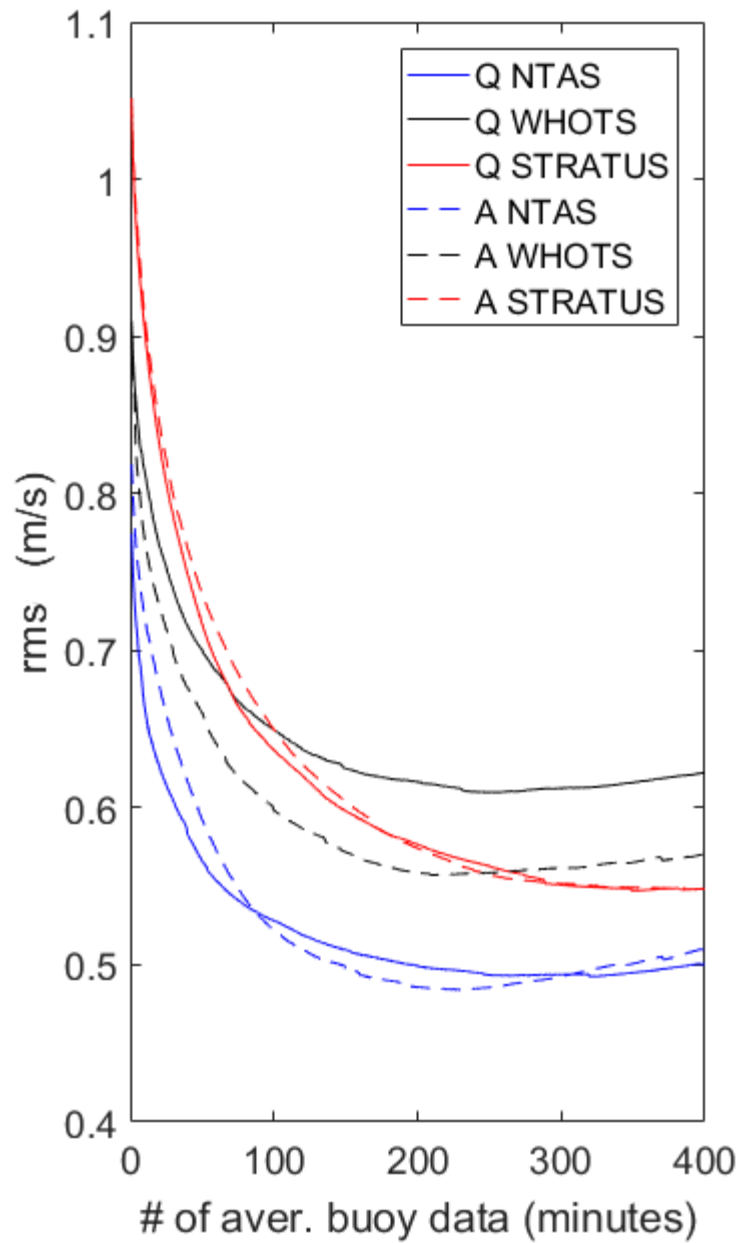
834   *Figure 4. Mean RMS between scatterometer and buoy against the averaging time of the buoy*

835   *data. Averaging times between one minute and 400 minutes were used with one minute*

836   *increments. Q refers to QuikSCAT and A refers to ASCAT.*
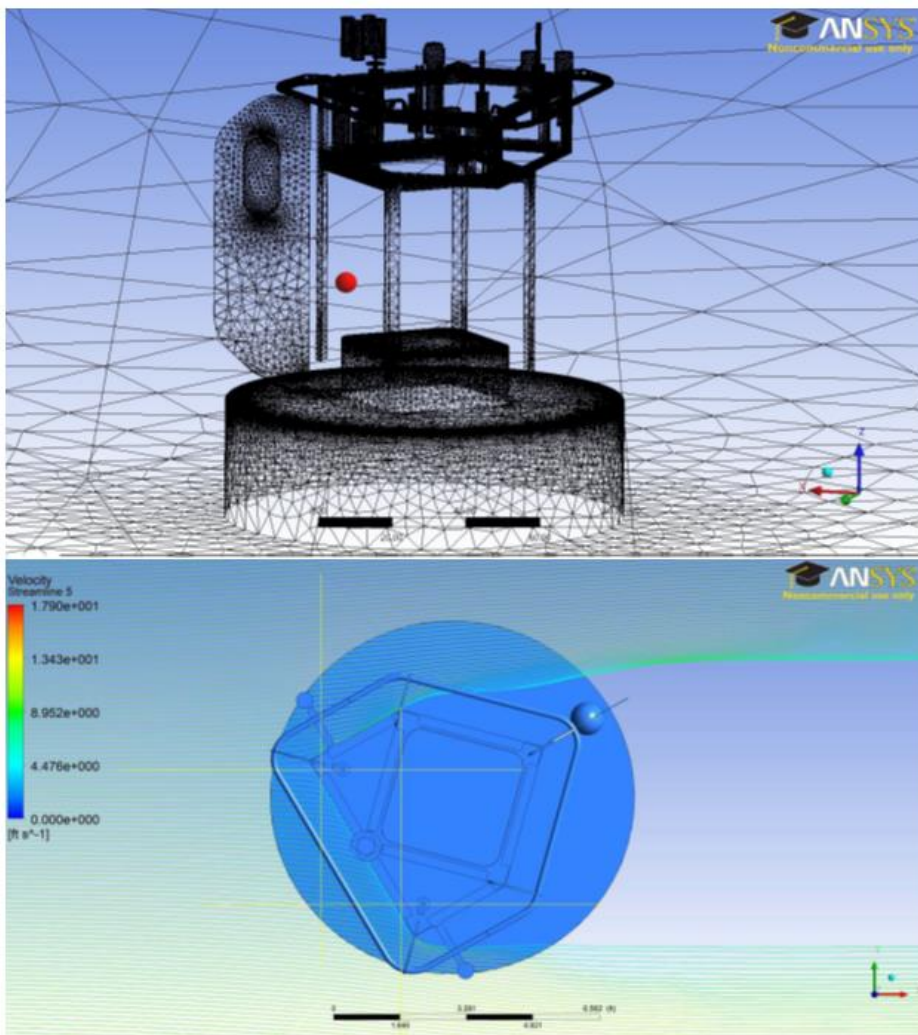
837

838 *Figure 5. (Upper panel) Model mesh of a WHOI buoy from the CFD study by* Emond *et al.* (2012).

839 *(Lower panel) Stream lines around the buoy from the same study (top view). The yellow crosses*

840 *are the wind sensor positions.*

841
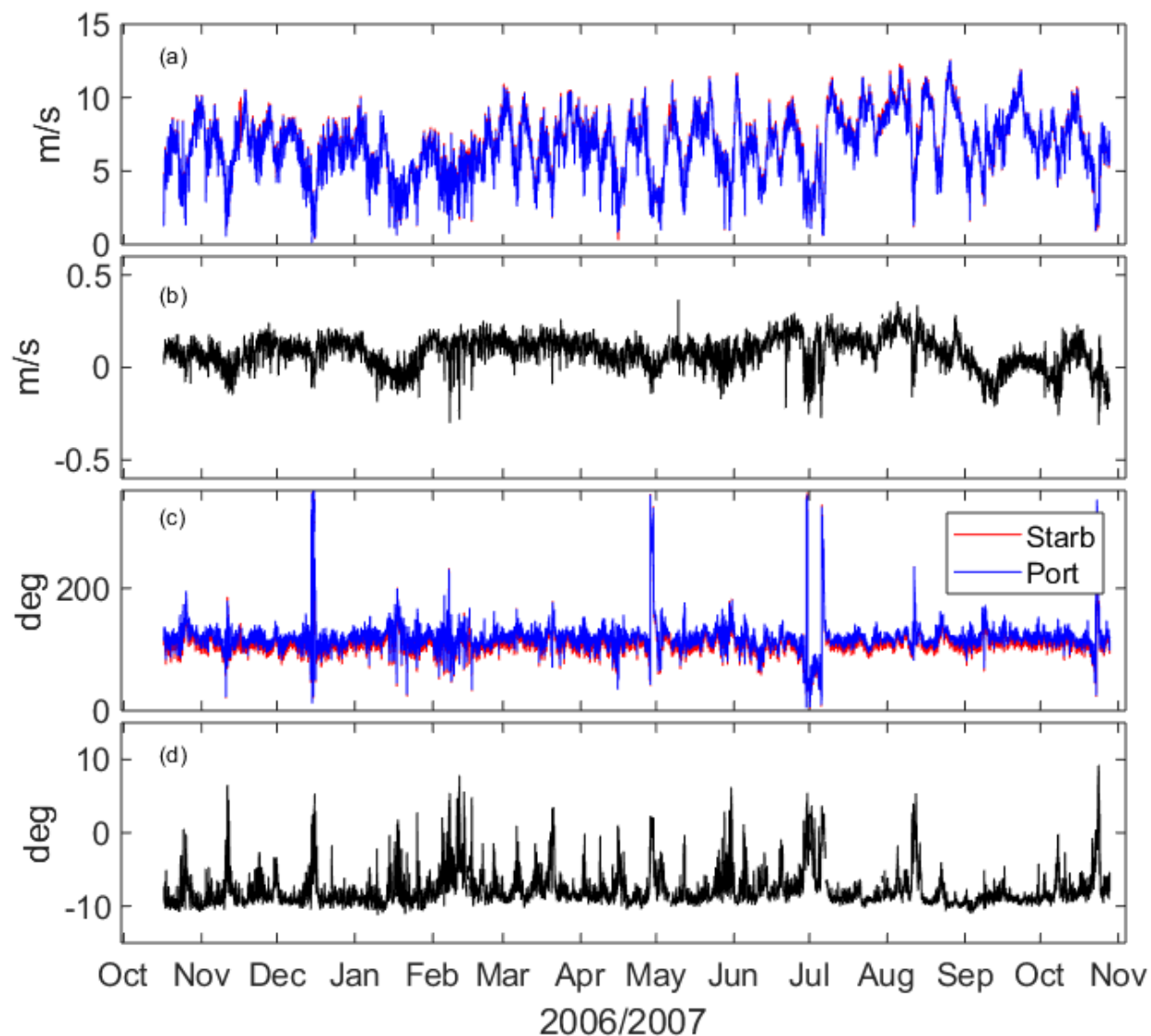
Figure 6. Time series of Stratus' seventh deployment. (a) Wind speed of starboard (red) and port

(blue) sensors, (b) the difference between them, (c) the wind direction of starboard (red) and

port (blue) sensors, and (d) the difference between them. Shown are one hour averages.
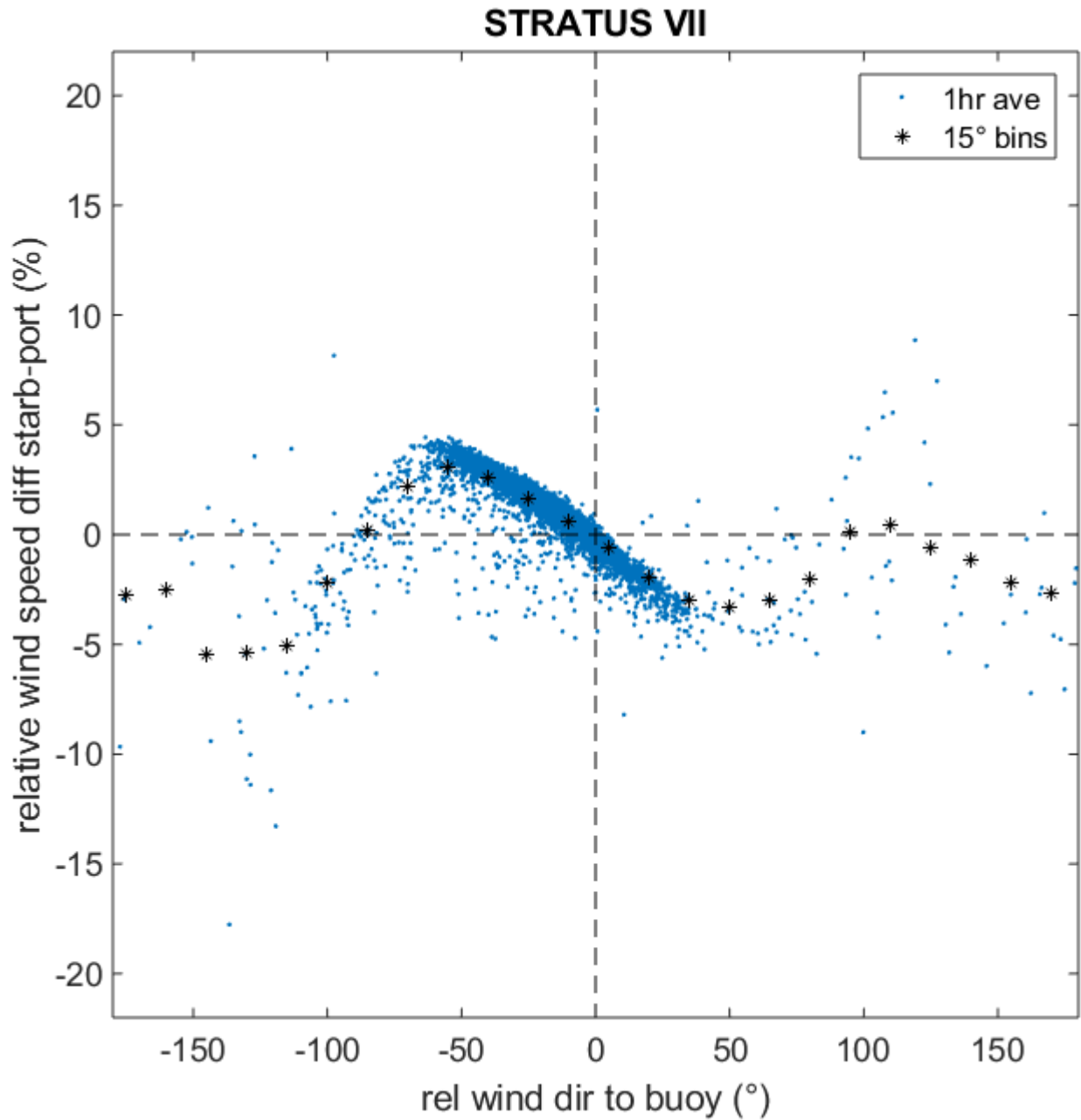
845

846   *Figure 7. Relative wind speed difference between starboard and port sensor for Stratus 7 against*

847   *relative wind direction. Shown are one hour averages (blue) and 15° bin averages (black stars).*

848
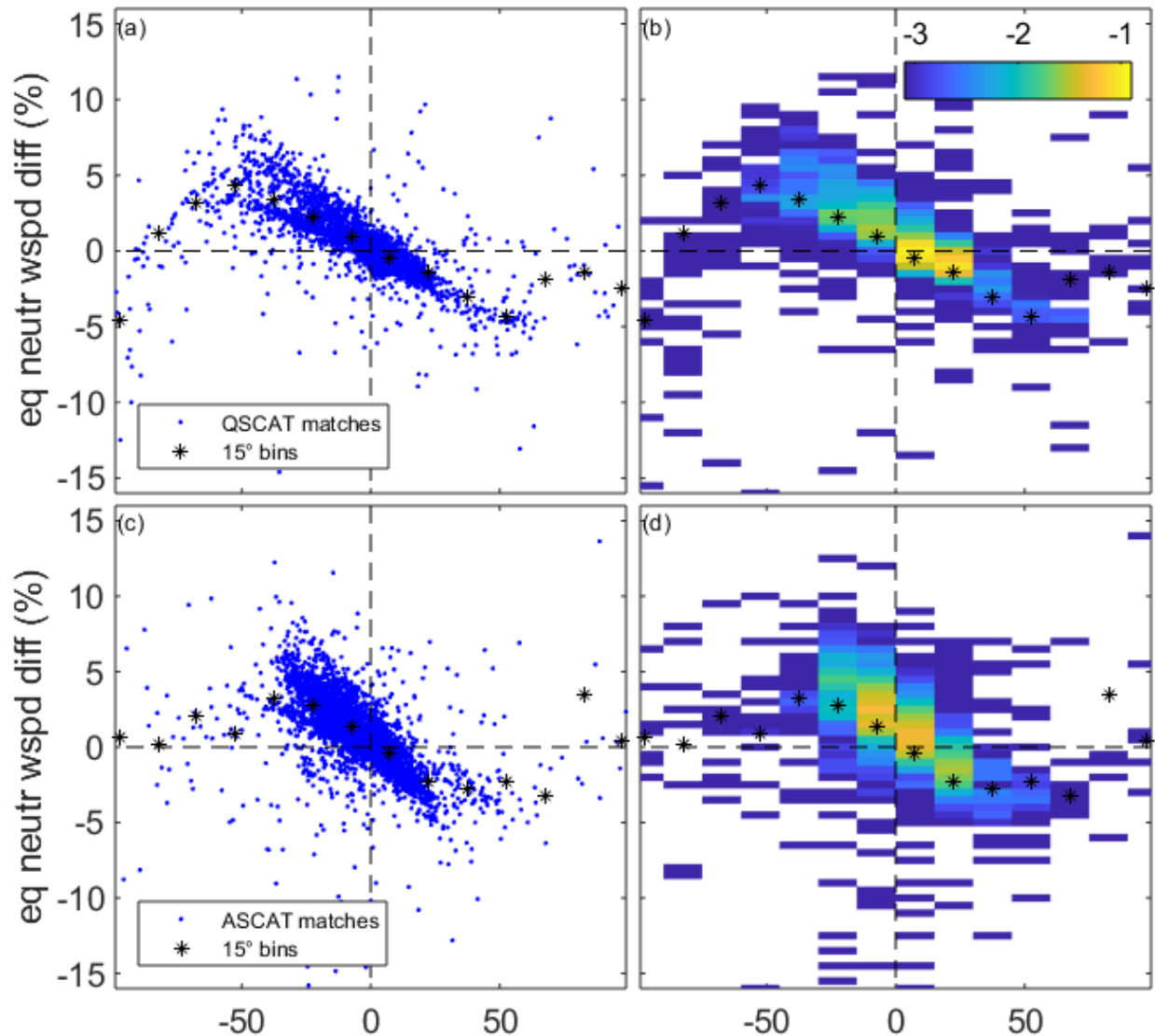
Figure 8. Equivalent neutral wind speed difference between the starboard and the port sensor in relative percentage and against the relative wind direction. (a) All data which match with QSCAT (blue) and the bin averages of all data (black stars). (b) Probability distribution of the QSCAT matches within 15° bins (colors; shown is the logarith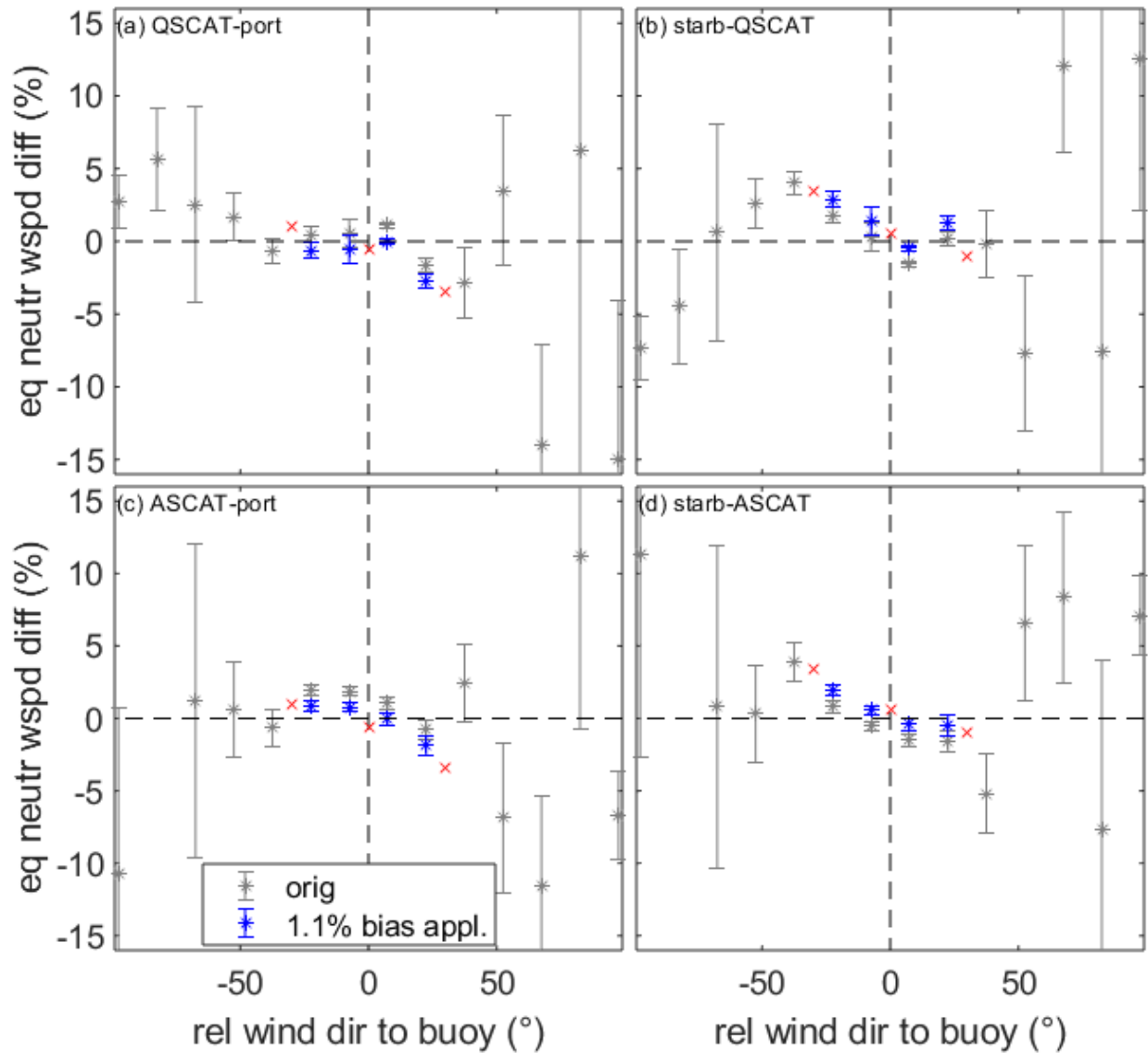m to base 10) and corresponding bin averages (black stars). (c) All data which match with ASCAT (blue) and the bin averages of all data (black stars). (d) Probability distribution of the ASCAT matches within 15° bins (colors; shown is the logarithm to base 10) and corresponding bin averages (black stars).

856

857   *Figure 9. Equivalent neutral wind speed differences, when replacing (a) the starboard module*

858   *with QSCAT, (b) the port module with QuikSCAT, (c) the starboard module with ASCAT, and (d)*

859   *the port module with ASCAT. Shown are the original bin averages (grey) and the bin averages*

860   *within ±30° with 1.1%-bias corrected satellite data (blue). The red crosses indicate the*

861   *theoretical flow distortion prediction as shown by* Emond *et al.* (2012)*.*
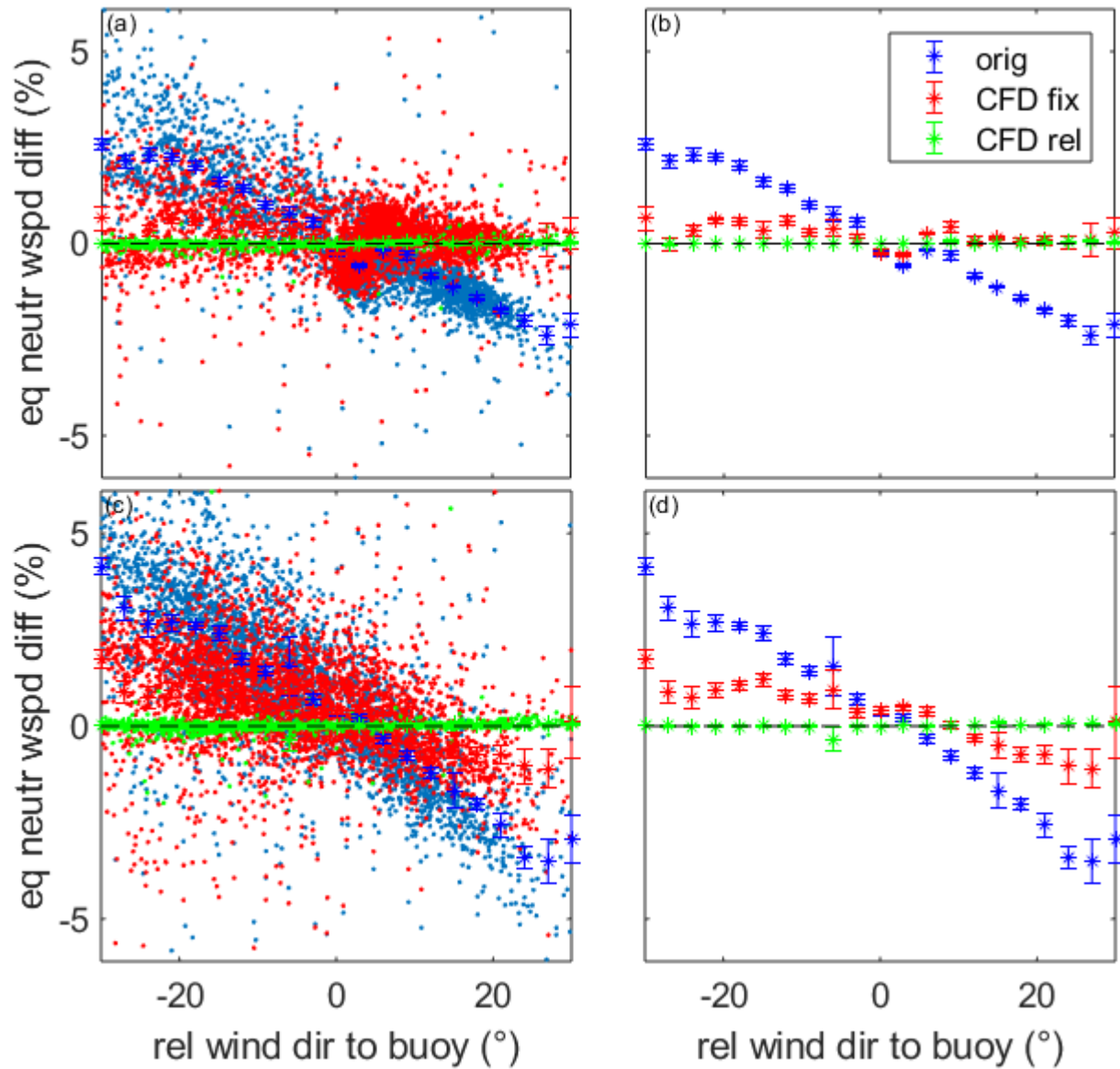
48

862

Figure 10. Equivalent neutral wind speed difference (starboard-port) from the QuikSCAT period:

(a) Data from Fig. 6a (blue), after the fixed correction (red), and after the relative correction

(green). (b) Corresponding bin averages from (a) with 3° bins. (c) The same as (a) for the ASCAT

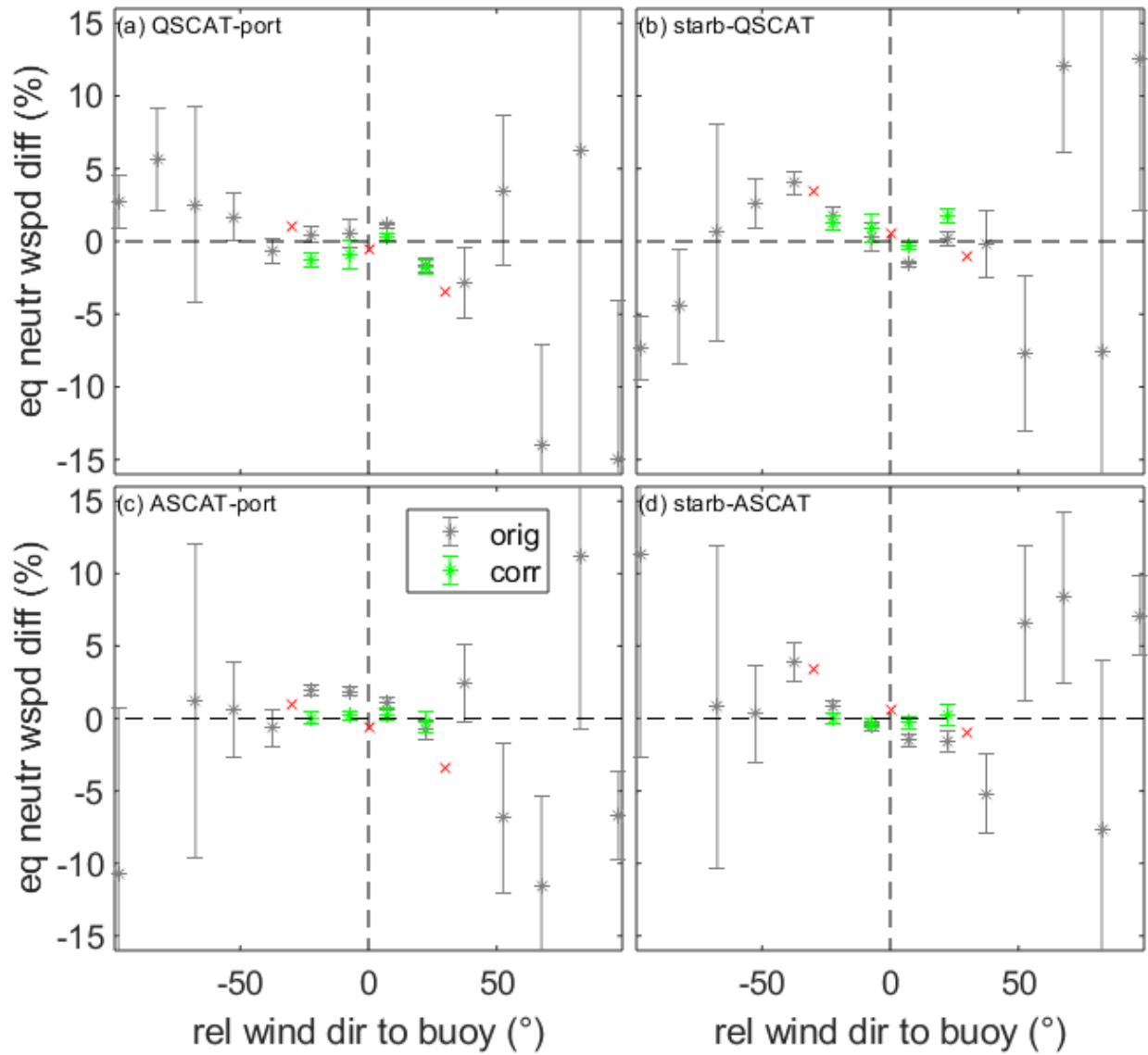*period and data from figure 6c (blue). (d) The same as (b) for the ASCAT period.*

49

867

868   *Figure 11. Same as figure 9, but with bias correction and relative flow distortion correction*

869   *(green). The red crosses indicate the theoretical flow distortion prediction as shown by* Emond *et*

870   *al. (2012).*